Macromolecules

Article

pubs.acs.org/Macromolecules

Lubrication by Polyelectrolyte Brushes

Ekaterina B. Zhulina[‡,§] and Michael Rubinstein*[,†]

[†]Department of Chemistry, University of North Carolina, Chapel Hill, North Carolina 27599-3290, United States

[‡]Institute of Macromolecular Compounds, Russian Academy of Sciences, Saint Petersburg 199004, Russia

[§]ITMO University, Saint Petersburg 197101, Russia

ABSTRACT: We develop a scaling model relating the friction forces between two polyelectrolyte brushes sliding over each other to the separation between grafted surfaces, number of monomers and charges per chain, grafting density of chains, and solvent quality. We demonstrate that the lateral force between brushes increases upon compression, but to a lesser extent than the normal force. The shear stress at larger separations is due to solvent slip layer friction. The thickness of this slip layer sharply decreases at distances on the order of undeformed brush thickness. The corresponding effective viscosity of the layer sharply increases from the solvent viscosity to a much higher value, but this increase is smaller than the jump of the normal force resulting in the drop of the friction coefficient. At stronger compression we predict the second sharp increase of the shear stress corresponding to interpenetration of the chains from the opposite brushes. In this regime the velocity-dependent friction coefficient between two partially interpenetrating polyelectrolyte brushes does not depend on the distance between substrates because both normal and shear forces are reciprocally proportional to the plate separation. Although lateral forces between polyelectrolyte brushes are larger than between bare surfaces, the enhancement of normal forces between opposing polyelectrolyte brushes with respect to normal forces between bare charged surfaces is much stronger resulting in lower friction coefficient. The model quantitatively demonstrates how polyelectrolyte brushes provide more effective lubrication than bare charged surfaces or neutral brushes.

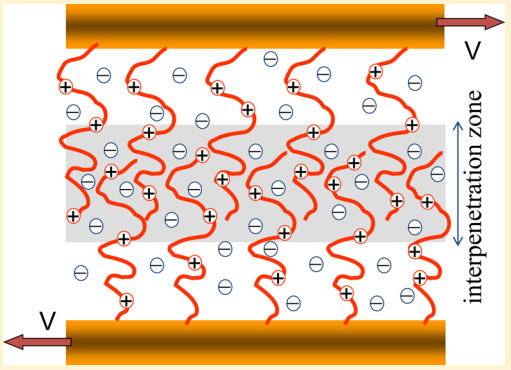

1. INTRODUCTION

Many processes in nature and technology involve polymer-decorated surfaces in liquid media, and therefore understanding of interactions between such surfaces is important from both academic and technological points of view. Dense grafting of polymer chains to a surface leads to the extension of these polymers due to interchain repulsions resulting in structures called polymer brushes.

Interactions between polymer brushes determine their effectiveness in steric stabilization, controlled by the normal forces between polymer-decorated surfaces. These interactions also determine friction between brushes, which is conventionally characterized by the friction coefficient, defined as the ratio of shear and normal forces between the two substrates sliding over each other. It was demonstrated experimentally that solid substrates decorated with charged polymer brushes have low friction coefficient when sheared against each other in polar solvents.[1] In contrast to sliding solid surfaces with typically velocity-independent friction coefficient, shear force between two surfaces with a liquid or brush layer between them increases with shear velocity. Since the friction coefficient of these sliding surfaces is velocity-dependent, the shear stress in this case is better described by the effective viscosity[2] defined as the ratio of shear stress and the effective shear rate.

The normal and shear forces between polymer-decorated surfaces were extensively studied over several decades.[1,3−15] The theoretical predictions for normal forces arising upon compression of neutral brushes were found to be in reasonable agreement with experiments and computer simulations.,[8,9,6] The Alexander−de Gennes scaling model of neutral brushes,[16,17] was generalized to incorporate the shear-induced deformation of tethered polymers in nonlinear response regime.[8]

The understanding of interactions between polyelectrolyte (PE) brushes is not as complete as between neutral ones. The Poisson−Boltzmann model of a pair of apposing PE brushes,[18,19] described the density profiles of polymer segments strongly coupled to the distribution of mobile counterions. The increase in normal force upon compression of apposing polyelectrolyte-decorated substrates is due to the increase of counterion concentration in the midplane between them (as there is no electric field at the midplane).[20] Since most counterions are confined within the brushes, the sharpest increase of the normal force upon compression occurs at the distance between grafted surfaces on the order of brush thickness. At this distance the concentration of counterions at the midplane changes from a very low value outside the brushes to a very high value inside the brushes.[19] One of the predictions of these works,[18,19] is the existence of a polymer-free gap filled with solvent and counterions between brushes compressed

Received: April 14, 2014
Revised: July 15, 2014
Published: August 5, 2014

   dx.doi.org/10.1021/ma500772a | Macromolecules 2014, 47, 5825−5838

against each other due to partial contraction of PE chains. The computer simulations[21] confirmed the shrinking of apposing PE brushes upon compression. The early theoretical studies[11,12] extended the scaling models[22,23] of PE brushes to analyze the change in conformations of tethered polyelectrolytes in strong flows under a constant normal load. They demonstrated the coupling between normal and shear forces due to tilting and stretching of polyions in apposing PE brushes in the direction of flow and predicted equilibrium distance between brush-decorated substrates as a function of shear and normal stresses.

In this paper we consider two planar substrates decorated with charged polymer brushes sliding over each other, and examine how the resulting shear force depends on length and degree of ionization of tethered polyelectrolytes, chain grafting density, and solvent quality. We demonstrate that charged polymer brushes enhance both normal and lateral forces between substrates in comparison to bare surfaces with equivalent charge densities. The normal force between strongly charged bare surfaces involves only distal Gouy−Chapman tails of counterions,[20] and is therefore much smaller than the normal force between compressed polyelectrolyte brushes separated by the same distance. The friction between bare charged surfaces is governed by the solvent viscosity and is also smaller than the friction between brushes at similar distances. We demonstrate that the enhancement of normal force by polyelectrolyte brushes with respect to bare charged surfaces is much larger than the corresponding increase of friction force resulting in lower friction coefficient between polyelectrolyte brushes. The behavior of polyelectrolyte brushes in salt-free solutions considered in this paper is also retained in solutions with added salt as long as counterion concentration is higher than that of salt ions. The mechanism of relatively low friction at high normal pressure maintained in polyelectrolyte brushes and gels sheds some light on lubrication phenomenon in biological systems, e.g., low friction at high load in synovial joints.

The rest of the paper is organized as follows. In section 2, we review the behavior of planar polyelectrolyte brushes immersed in a salt-free solvent (section 2.1), the normal force between a pair of polyelectrolyte brushes (section 2.2) and their interpenetration (section 2.3). Our results on the friction between polyelectrolyte brushes are presented in section 3 and compared with the friction between bare charged surfaces in section 4. In section 5, we formulate the conclusions. In the Appendix, we estimate the solvent penetration length for neutral brushes and for PE brushes in the osmotic regime.

2. POLYELECTROLYTE BRUSHES

2.1. Single Brush. Properties of a single planar polyelectrolyte (PE) brush in contact with a salt-free solution depend on the following parameters: (i) contour length Nb where N is the number of Kuhn segments of length b, (ii) degree of chain ionization f (fraction of charged Kuhn segments), (iii) Bjerrum length l_B defined as the distance at which two elementary charges e interact with thermal energy $k_BT = e^2/(\varepsilon l_B)$ in a solvent with dielectric constant ε, (iv) grafting density ρ (number of chains tethered per unit surface area). Each polyion has fN elementary charges e uniformly distributed along its backbone, and the same number fN of mobile monovalent counterions distributed in solution above the grafted surface (both inside the brush and outside it). We assume relatively low charge density along the chain (less than one charge per Bjerrum length, or $l_B < bf^{-\nu}$). Brushes with higher charge density and the resulting Manning condensation of counterions are considered in section 5. Nonelectrostatic interactions between monomers determine local chain statistics: size $r \simeq bg^{\nu}$ for a small chain section with g Kuhn monomers with exponents $\nu \approx 3/5$ and $\nu = 1/2$ for good and Θ solvent conditions, respectively.

Free Chain in a Dilute Solution. Balancing Coulomb electrostatic energy

$$W \simeq k_BTl_B\frac{(fN)^2}{L} \tag{1}$$

of a polyion with end-to-end distance L and backbone elastic free energy[24]

$$F_{elastic} \simeq k_BT\left(\frac{L}{bN^{\nu}}\right)^{1/(1-\nu)} \tag{2}$$

leads to the average end-to-end distance of a polyion in a dilute salt-free solution,[25]

$$L \simeq bN(uf^2)^{(1-\nu)/(2-\nu)} \tag{3}$$

where we define the dimensionless ratio u of Bjerrum length l_B and Kuhn length b

$$u = \frac{l_B}{b} = \frac{e^2}{k_BT\varepsilon b} \tag{4}$$

The exponent of the effective interaction parameter uf^2 in eq 3 is 1/3 in a Θ solvent with $\nu = 1/2$, and 2/7 in a good solvent with $\nu = 3/5$. A single polyion can be envisioned as a stretched string of N/g_e electrostatic blobs with size

$$\xi_e \simeq b(uf^2)^{-\nu/(2-\nu)} \tag{5}$$

containing

$$g_e \simeq (uf^2)^{-1/(2-\nu)} \tag{6}$$

monomers each. On length scales smaller than ξ_e, the electrostatic energy is less than thermal energy k_BT, and the local chain statistics is almost unperturbed ($\xi_e \simeq bg_e^{\nu}$). On length scales larger than ξ_e, polyion is stretched by electrostatic repulsion between charges, and its end-to-end distance in a salt-free solution is $L \simeq \xi_eN/g_e$ (see eq 3).

Charged Mushroom (CM) Regime. If polyions are sparsely tethered to the substrate, with grafting density $\rho \ll L^{-2}$, the grafted layer is considered to be in charged mushroom (CM) regime with characteristic end-to-end distance of chains given by eq 3. In contrast to neutral grafted chains in mushroom regime, polyelectrolytes in charged mushroom (CM) regime interact with each other. This long-range interaction can result in their orientation perpendicular to the grafted surface. The electric field due to grafted chains with charge efN on each creates surface charge density $efN\rho$ and electric field in solvent with dielectric constant ε

$$E \simeq efN\rho/\varepsilon = kTl_Bf N\rho/e \tag{7}$$

This field imposes a force on each grafted chain

$$efNE \simeq (efN)^2\rho/\varepsilon = kTl_B(fN)^2\rho \tag{8}$$

The energy gain due to orienting chain perpendicular to the grafted surface (along the field) is on the order of the product of this force and chain size L (see eq 3)

$$U_{elec} \approx k_BTl_B(fN)^2\rho L \tag{9}$$

dx.doi.org/10.1021/ma500772a | Macromolecules 2014, 47, 5825−5838

which is the energy cost of rotating one chain in the electric field of other grafted chains by an angle on the order of unity. The onset of the orientation occurs at grafting densities ρ_{orient} at which this electrostatic orientation energy per chain U_{elec} is on the order of thermal energy k_BT. This onset of grafted polyelectrolytes, orienting each other in the CM regime, occurs at

$$\rho_{orient} \simeq \frac{1}{l_B(fN)^2L} \tag{10}$$

At lower grafting densities $\rho < \rho_{orient}$, tethered polyelectrolytes are almost noninteracting and freely rotating. At higher grafting densities $\rho > \rho_{orient}$, intermolecular interaction (eq 9) is strong enough to orient polyelectrolytes primarily perpendicular to the grafted surface, but not strong enough to deform them significantly. At these grafting densities, the intramolecular electrostatic repulsion (eq 1) is much stronger than the intermolecular one and controls chain extension (see the first plateau in Figure 1). This crossover grafting density at

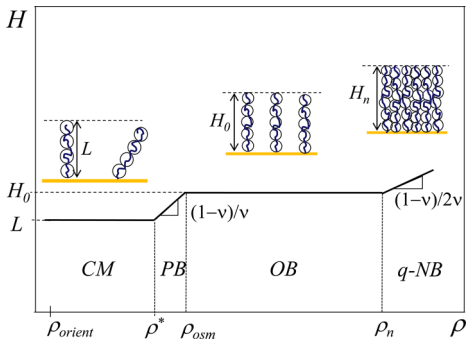

Figure 1. Schematic dependence of PE brush thickness H on chain grafting density ρ in logarithmic coordinates.

which the intermolecular electrostatic interaction energy (eq 9) becomes on the order of the intramolecular one (eq 1) corresponds to the separation between chains on the order of their size L (eq 3),

$$\rho^* \simeq L^{-2} \tag{11}$$

In contrast to tethered neutral chains, the crossover between charged mushroom and charged brush regimes occurs prior to the overlap of chain projections onto grafted surface. Note that for polyions elongated by the intramolecular Coulomb repulsions between charged monomers $\rho_{orient} \ll \rho^*$.

Pincus Brush (PB) Regime. At higher grafting densities $\rho > \rho^*$ tethered polyions create an electric field E (eq 7) which stretches each chain beyond the size of a free polyion L (eq 3). The size of the chain in this regime is determined by the balance of the electrostatic energy per chain (eq 9 with L replaced by H)

$$U_{elec} \simeq k_BTl_B(fN)^2\rho H \tag{12}$$

and elastic free energy per chain (eq 2 with L replaced by H)

$$F_{elast} \simeq k_BT\left(\frac{H}{bN^\nu}\right)^{1/(1-\nu)} \tag{13}$$

resulting in the brush height

$$H \simeq L(\rho L^2)^{(1-\nu)/\nu} \simeq b(uf^2\rho b^2)^{(1-\nu)/\nu}N^{(2-\nu)/\nu} \tag{14}$$

increasing with grafting density ρ linearly in a Θ solvent and with exponent 2/3 in a good solvent (see Figure 1). This regime of unscreened electrostatics (referred to as Pincus regime) continues as long as counterions are able to escape from the brush. The counterion confinement length Λ (called Gouy−Chapman length) is defined as the distance at which the energy of counterion attraction to the charged surface is higher than that at the surface by the thermal energy k_BT. Half of all counterions are located within the Gouy−Chapman length[20]

$$\Lambda = 1/(2\pi l_B fN\rho) \tag{15}$$

from the charged surface. The upper boundary of the Pincus regime corresponds to $\Lambda = H$ or to the grafting density

$$\rho_{osm} \simeq (l_BbN^2f^{2-\nu})^{-1} \simeq (l_BfNH_0)^{-1} \tag{16}$$

where H_0 is the thickness of the brush with grafting density at or above the crossover value ρ_{osm} (see eq 17 below). Note that Pincus regime ($\rho^* < \rho < \rho_{osm}$) exists only for weakly charged grafted polyions with $bf^{-\nu} > l_B$, while for strongly charged polyelectrolytes ($bf^{-\nu} < l_B$) with condensed counterions there is no Pincus regime and $\rho^* \simeq \rho_{osm}$ (see section 5).

Osmotic Brush (OB) Regime. At higher grafting densities $\rho > \rho_{osm}$, counterions become localized within the brush, and their entropy (osmotic pressure) dominates the brush properties. This main regime of polyelectrolyte brushes is called osmotic brush (OB) regime. Here, the size of the brush is determined by the balance of the osmotic pressure of counterions, trying to maximize their entropy by increasing the brush volume, and the elasticity of tethered chains opposing this tendency. The balance of the two forces corresponds to both, osmotic and elastic parts of the free energy per chain ~ fNk_BT, independent of the grafting density. Therefore, the scaling model[22,23] predicts the brush thickness in this osmotic regime

$$H_0 \simeq bNf^{1-\nu} \tag{17}$$

to be independent of the grafting density ρ (see the second plateau in Figure 1). The chain size H_0 in the osmotic brush regime of weakly charged polyions (with $bf^{-\nu} > l_B$) is strongly stretched compared to its free polyelectrolyte size L with effective tension blobs[24] containing one elementary charge and consisting of $g_P \approx 1/f$ monomers of size

$$\xi_P \approx bf^{-\nu} \tag{18}$$

Thus, the size of the stretched chain (and the thickness of the osmotic brush) is $H_0 \approx \xi_P N/g_P$ (see eq 17).

Quasi-Neutral Brush (q-NB) Regime. At very high grafting densities

$$\rho > \rho_n \simeq b^{-2}f^{2\nu} \tag{19}$$

the distance between chains $\rho^{-1/2}$ becomes smaller than the Pincus blob size ξ_P (eq 18) and the energy of short-range excluded volume interactions between monomers becomes higher than the counterion osmotic contribution to the brush free energy. For these very high grafting densities $\rho > \rho_n$ tethered polyions enter the quasi-neutral brush (q-NB) regime. PE brushes in q-NB regime have the same properties as neutral brushes. The thickness of a neutral brush is determined by the balance of short-range excluded volume repulsion and chain elasticity. It can be estimated by the Alexander−de Gennes scaling model[16] as the length of a stretched array of correlation blobs with the size of each blob on the order of the distance

dx.doi.org/10.1021/ma500772a | Macromolecules 2014, 47, 5825−5838

between grafting points, $\xi_n = \rho^{-1/2}$. The number of correlation blobs per chain is $N/g_n = N(\rho b^2)^{1/(2\nu)}$, and the brush thickness increases with grafting density as

$$H_n \simeq \xi_n N/g_n \simeq bN(\rho b^2)^{(1-\nu)/(2\nu)} \tag{20}$$

Figure 1 shows the increase in brush thickness H with grafting density ρ in this quasi-neutral regime with the scaling exponent $(1-\nu)/(2\nu)$ which is half of the exponent in the Pincus brush regime. In Θ solvent with $\nu = 1/2$, the exponent $(1-\nu)/(2\nu) = 1/2$ while in good solvent with $\nu = 3/5$ the exponent $(1-\nu)/(2\nu) = 1/3$.

Parabolic Molecular Field. In the Alexander–de Gennes model of neutral brushes,[16,17] all chain ends are assumed to be located in the outmost blob, and the density is assumed to be uniform throughout the brush. In more sophisticated models of neutral brushes,[26−28] chain ends are distributed throughout the brush in such a way that the effective molecular field acting on chain segments is parabolic. This results in the almost parabolic density profile of solvated neutral brushes in good solvents.

As in neutral brushes, the molecular field in polyelectrolyte brushes with fractional charge ef per Kuhn monomer is also almost parabolic.[19] However, this field in the charged brushes is essentially electrostatic acting on the charged monomers. Therefore, the electrostatic potential inside a polyelectrolyte brush is parabolic, resulting in the Gaussian distribution of counterions, as dictated by the Boltzmann law.[19] This parabolic electrostatic potential is produced by the combined electric charges of both tethered polyions and counterions. The parabolic shape of the electrostatic potential indicates that electric field (derivative of the electrostatic potential) in the brush increases linearly with the distance from the grafted surface. Linear increase of the electric field implies by the Gauss law that the net charge density in the brush is uniform. This net charge density is the difference between charges on the chains and counterions. Therefore, the polymer density profile follows that of counterions and is also Gaussian to ensure that the difference between counterion and polymer charge profiles is distance-independent. Since the net charge of the brush is not exactly zero, the compensating counterions (Δn per chain) escape from the brush and form Gouy–Chapman layer of thickness λ. These escaped counterions create a capacitor with characteristic thickness $H_0 + \lambda$ and the escaped charge $e\Delta n$ is related to Gouy–Chapman length λ (cf. eq 15) outside the brush

$$\lambda \simeq (l_B \rho \Delta n)^{-1} \tag{21}$$

The electrostatic energy per unit area of this capacitor

$$F_{elect} \simeq k_B T l_B \rho^2 \Delta n^2 (H_0 + \lambda) \tag{22}$$

is balanced by the entropic part of free energy per unit area gained by escaped counterions

$$F_{ent} \simeq k_B T \rho \Delta n \ln(c_{out}/c_0) \tag{23}$$

with concentration $c_0 = fN\rho/H_0$ of ions inside the brush and concentration of ions $c_{out} = \Delta n\rho/\lambda$ in the Gouy–Chapman layer. This balance leads to the width of Gouy–Chapman layer λ comparable to the polyelectrolyte brush thickness H_0 in the osmotic regime (eq 17)

$$\lambda \simeq H_0 \tag{24}$$

up to logarithmic correction on the order of $\ln(c_0/c_{out})$.

The net number of charges escaped from the brush per unit area is therefore reciprocally proportional to the product of the brush thickness H_0 and Bjerrum length l_B,

$$\rho \Delta n \simeq (l_B H_0)^{-1} \tag{25}$$

Note that the concentration of counterions in the Gouy–Chapman layer outside the brush, $c_{out} = \rho\Delta n/\lambda \simeq \rho^2 l_B \Delta n^2 \simeq (l_B H_0^2)^{-1}$, is much smaller than concentration of counterions inside the brush, $c_0 = fN\rho/H_0$, in the osmotic regime, $\rho \gg \rho_{osm}$, with the ratio of the two concentrations (see eq 16)

$$\frac{c_0}{c_{out}} \simeq \frac{fN\rho/H_0}{(l_B H_0^2)^{-1}} \simeq \frac{H_0}{\Lambda} \simeq \frac{\lambda}{\Lambda} \simeq \frac{\rho}{\rho_{osm}} \gg 1 \tag{26}$$

determined by how deep the brush is inside the osmotic regime ρ/ρ_{osm}. We emphasize the difference between Gouy–Chapman length Λ due to all charges (eq 15) and Gouy–Chapman length λ due only to charges Δn escaped from the brush (eq 21).

We estimate the boundaries between different PE brush regimes using the values of parameters close to those in[14] For grafted polyelectrolyte chains with $N = 200$ Kuhn monomers of length $b \approx l_B = 0.7$ nm, and degree of ionization $f = 0.5$ one finds crossover surface densities: $\rho_{orient} \simeq 2 \times 10^{-8}$ nm^{-2}, $\rho^* \simeq 1.3 \times 10^{-4}$ nm^{-2}, $\rho_{osm} \simeq 1.4 \times 10^{-4}$ nm^{-2}, and $\rho_n \simeq 1$ nm^{-2}. Note that the experimentally relevant and the widest range of surface densities of grafted chains corresponds to the osmotic regime. For example, the experimentally studied surface density of grafted chains[14] $\rho \approx 0.2$ nm^{-2} is in the osmotic regime of PE brush with predicted brush thickness $H_0 \simeq 100$ nm much larger that the "bare" Gouy–Chapman length $\Lambda \simeq 0.01$ nm and therefore with very large ratio $c_{inside}/c_{outside} \simeq H_0/\Lambda \simeq 10^4$. Below we consider polyelectrolyte brushes prepared in this main (OB) regime. Note that upon strong compression they could enter the quasi-neutral regime.

2.2. Normal Force between a Pair of Polyelectrolyte Brushes. The main focus of this paper is on the interactions between two polyelectrolyte brushes. In contrast to neutral brushes, polyelectrolyte brushes repel each other at distances D between grafted surfaces much larger than twice the thickness H_0 of each brush. The source of this long-range interaction is the confinement of counterions in the space between two surfaces. The free energy of dissociated counterions is dominated by their translational entropy, which is much larger than interaction part of their free energy. The self-energy of counterions does not change upon brush deformation and therefore does not contribute to the variation of free energy.

The resulting pressure P felt by the surfaces is given by Van't Hoff (ideal gas-like) law for counterion density $c_i(D/2)$ in the middle of the gap, $P = k_B T c_i(D/2)$. At distances between grafted surfaces $D \gg \lambda \simeq H_0$, the pressure

$$P = k_B T c_i(D/2) \simeq \frac{k_B T}{l_B D^2} \text{ weak compression}, \quad D \gg H_0 \tag{27}$$

is determined by the "tail" of the Gouy–Chapman counterion distribution, $c_i(z) \approx (l_B z^2)^{-1}$ at distance $z = D/2$. Note that this pressure is independent of brush parameters and depends only on the separation D between grafted surfaces and Bjerrum length l_B (for monovalent counterions).

At stronger compressions, $D < H_0$, counterions are distributed almost uniformly between the two grafted surfaces with concentration $c_i = 2fN\rho/D$, and produce osmotic pressure

dx.doi.org/10.1021/ma500772a | Macromolecules 2014, 47, 5825−5838

$$P \approx k_B T c_i \simeq \frac{k_B T f N \rho}{D} \text{ strong compression}, \quad D < H_0 \tag{28}$$

Note that there is sharp crossover between these two expressions, eqs 27 and 28, with rapidly increasing pressure from a low value of $kT/(l_B H_0^2)$ to a high value of $kTc_0 \simeq kTfN\rho/H_0$ by a large factor $fN\rho H_0 l_B \simeq \lambda/H_0$ upon the decrease of separation D by the factor on the order of unity (for example, from $D = 2H_0$ to $D = H_0$) as depicted in Figure 2. The crossover between two asymptotic dependences of osmotic pressure (lines with slopes −2 and −1 given by respective eqs 27 and 28) is indicted by the vertical dashed line.

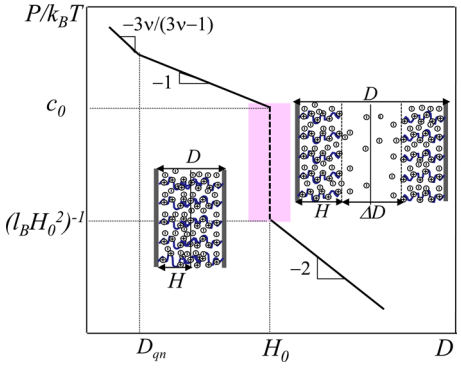

Figure 2. Normal force per unit area in compressed osmotic PE brushes as a function of distance D between surfaces in logarithmic coordinates. $c_0 = fN\rho/H_0$. The interval of D with a sharp increase in force is shadowed pink.

The normal force between compressed polyelectrolyte brushes is dominated by counterions (eq 28) as long as there is more than one free counterion per correlation volume. The normal pressure at higher compression is controlled by direct interactions between polymer chains and is similar to the pressure in neutral brushes (see eqs 38 and 39 below)

$$P \approx (k_B T/b^3)(cb^3)^{3\nu/(3\nu-1)} \text{ quasi-neutral}, \quad D < D_{qn} \tag{29}$$

where c is the monomer number density $c = 2N\rho/D$.

2.3. Interpenetration of Polyelectrolyte Brushes. In contrast to neutral brushes, polyelectrolyte brushes contract upon compression leaving the gap of width $\Delta D = D - 2H$ filled with solvent and counterions.[19] Therefore, there is a regime of intermediate compression without physical contact and interpenetration of monomers from apposing brushes. This gap acts as a lubrication layer upon shear of apposing brushes at distances between plates $D > L$ larger than the size of a free polyion (eq 3).

At smaller separations between surfaces $D < L$, polyions penetrate into apposing brushes up to characteristic distance, called penetration length δ.

The polymer penetration length δ_n in neutral brushes with parabolic molecular field was estimated in refs 29 and 30

$$\delta_n \simeq \frac{b^{4/3} N^{2/3}}{H^{1/3}} \tag{30}$$

It increases upon brush compression (a decrease in brush thickness $H = D/2$). Equation 30 is applicable for chains with Gaussian elasticity in both dry (solvent-free) and solvated neutral brushes. It can also be applied to compressed polyelectrolyte brushes on scales larger than correlation length ξ, as we demonstrate below (see eq 34).

At strong compressions $D \ll L$, polyelectrolyte chains uniformly fill the space between grafted surfaces similar to semidilute salt-free polyelectrolyte solution with concentration $c = 2N\rho/D$ and correlation length[31,32]

$$\xi \simeq (cb)^{-1/2} (uf^2)^{-(1-\nu)/(4-2\nu)} \tag{31}$$

This solution could be envisioned as densely packed melt of correlation blobs with size ξ. At distances r smaller than correlation length ξ, polyelectrolytes retain the extended conformations of dilute solution polyions, and blob size ξ is related to the number of monomers g in the blob according to eq 3

$$\xi \simeq bg(uf^2)^{(1-\nu)/(2-\nu)} \tag{32}$$

At larger distances $r \gg \xi$ polyions are envisioned as Gaussian chains of N/g correlation blobs each. The end-to-end distance of unconstrained polyions in a semidilute polyelectrolyte solution is[32]

$$R \simeq \xi\sqrt{N/g} \simeq \frac{bN^{1/2}}{(cb^3)^{1/4}} (uf^2)^{(1-\nu)/(8-4\nu)} \tag{33}$$

which is on the order of the fluctuation size of a polyelectrolyte chain at this concentration.

We distinguish two cases for a pair of apposing polyion brushes in strongly compressed regime ($D < L$) depending on the separation between grafted surfaces D in comparison to this fluctuation size R (eq 33). If $R < D < L$ the grafted chains are stretched in comparison to their "happy" fluctuation size ($H > R$) and the interpenetration between apposing brushes is only partial ($\delta < H$). If the separation between plates is smaller than the fluctuation size $D = 2H < R$ the grafted chains are compressed and the two brushes fully interpenetrate ($\delta \approx H$).

2.3.1. Partial Interpenetration. In a compressed polyelectrolyte brush with thickness H in the interval $R < H < L$, the chains of blobs of size ξ each are stretched in the normal direction. To optimize their free energy, tethered polyions distribute free ends throughout the slit between surfaces with partial penetration into apposing brush. Similarly to dry (solvent-free) brush of neutral polymers, tethered chains of correlation blobs experience parabolic potential, and interpenetration length δ for polyions can be found by substituting $b \to \xi$ and $N \to N/g$ and $H = D/2$ in eq 30 to give

$$\delta \simeq \frac{\xi^{4/3}(N/g)^{2/3}}{D^{1/3}} \simeq \frac{R^{4/3}}{D^{1/3}} \tag{34}$$

Note that fluctuation size R of polyelectrolyte chain in solution (eq 33) decreases with concentration c as $R \sim c^{-1/4} \sim D^{1/4}$. Therefore, interpenetration width δ in eq 34 is independent of spacing D between plates in the regime of partial interpenetration. In the case of weak interpenetration $\delta \ll D$, only a small fraction δ/D of all monomers is in the interpenetration zone. The total number of blobs per unit area in the interpenetration zone is $n_B = \delta/\xi^3$ with $n_B/2$ from each brush. Each chain section in the interpenetration zone is almost unstretched with $(\delta/\xi)^2$ blobs per section. The number of chain sections per unit area in the interpenetration zone $1/(\delta\xi)$ is smaller than the total grafting density $\rho = D/(\xi^3 N/g)$ by the factor

dx.doi.org/10.1021/ma500772a | Macromolecules 2014, 47, 5825−5838

$$\xi^2(N/g)/(\delta D) \simeq R^2/(\delta D) \simeq (\delta/D)^{1/2} \quad (35)$$

where we used eqs 33 and 34, $\xi^2 N/g \simeq R^2 \simeq \delta^{3/2} D^{1/2}$. Therefore, the fraction of polyions with free ends in the interpenetration zone is $(\delta/D)^{1/2}$, while the fraction of monomers in this zone δ/D, leading to the average number of monomers per chain section in the interpenetration zone $N(\delta/D)^{1/2}$.

2.3.2. Full Interpenetration. A decrease in spacing between plates D eventually results in the full interpenetration of apposing brushes, $\delta \simeq D$, at plate separation $D \simeq R$. At smaller distances $D < R$, there is full interpenetration of apposing brushes, $\delta = D$, with total number of "interpenetrating" blobs per unit area $n_B = D/\xi^3$ where blob size ξ is given by eq 31.

At distances D between plates smaller than

$$D_n \simeq b^3 N\rho(uf^2)^{-(3\nu-1)/(2-\nu)} \simeq \rho b^2 L(uf^2)^{-2\nu/(2-\nu)} \quad (36)$$

the correlation length ξ in compressed polyelectrolyte brushes is governed by the nonelectrostatic interactions,

$$\xi \simeq b(cb^3)^{-\nu/(3\nu-1)} \quad (37)$$

As long as there are many counterions (with translational entropy $\simeq k_B T$ each) per correlation blob with size ξ (eq 37), the normal force P is dominated by the osmotic pressure of counterions. This mixed regime with correlation length controlled by nonelectrostatic interactions (eq 37), but osmotic pressure dominated by counterions is expected in the interval of distances between surfaces $D_{qn} < D < D_n$. At the lower boundary of this interval

$$D_{qn} \simeq b^3 \rho N f^{1-3\nu} \quad (38)$$

there is one counterion per correlation volume. At even stronger compressions with $D < D_{qn}$, the number of counterions per correlation blob becomes smaller than unity. Here, both correlation length ξ and osmotic pressure

$$P \simeq \frac{k_B T}{\xi^3} \simeq \frac{k_B T}{b^3}(cb^3)^{3\nu/(3\nu-1)}, \quad \text{for } D < D_{qn} \quad (39)$$

are determined by the nonelectrostatic interactions between monomers. In this interval of plate separations ($D < D_{qn}$), compressed polyelectrolyte brushes behave as quasi-neutral ones.

3. FRICTION BETWEEN POLYELECTROLYTE BRUSHES

3.1. Bare Surfaces. Before describing the effect of PE brushes on the friction between substrates, consider the friction between bare planar surfaces with charge number density $Nf\rho$ immersed in a Newtonian liquid with viscosity η_s. We assume that shear does not perturb the Gouy−Chapman counterion distribution. The normal force P is determined by the counterion pressure in the middle of the gap between surfaces[20]

$$P = k_B T c_{ion}(D/2) \simeq k_B T \begin{cases} (l_B D^2)^{-1} & D \gg \Lambda \\ (l_B D\Lambda)^{-1} \simeq Nf\rho/D & D \ll \Lambda \end{cases} \quad (40)$$

The shear stress σ_{bare} (friction force per unit area) experienced by planar surfaces in laminar flow with effective velocity gradient V/D equal to the actual strain rate

$$\dot{\gamma} = dV/dz = V/D \quad (41)$$

is

$$\sigma_{bare} = \eta_s \dot{\gamma} \quad (42)$$

Therefore, in the case of bare surfaces the effective viscosity defined as the ratio of measured shear stress σ and externally imposed effective shear rate V/D

$$\eta_{eff} \equiv \frac{\sigma D}{V} = \frac{\sigma_{bare}}{\dot{\gamma}} = \eta_s \quad (43)$$

is equal to the solvent viscosity η_s.

3.2. Polyelectrolyte Brushes. The shear of polymer-covered substrates with a low sliding velocity V results in linear velocity dependence of shear stress (friction force per unit area) $\sigma \sim V$. Velocity V in this linear regime is low enough to allow complete relaxation of polyion conformations with almost unperturbed distribution of monomers in PE brush in both normal and lateral directions.

3.2.1. Regime of Weak Compression ($D \gg H_0$). In the case of weak compression there is a gap between brushes acting as a lubrication layer. The flow of solvent within the brush is suppressed on hydrodynamic screening length scale ξ_h much smaller than PE brush thickness H_0. The shear-induced laminar flow of the solvent is therefore limited to the gap of thickness $D - 2H + 2\xi_h = \Delta D + 2\xi_h$, where ξ_h is the flow penetration length into each of the brushes. The thickness of this gap is estimated in the Appendix for the polyions with the Gaussian elasticity. The shear stress σ_{brush} is obtained in this regime of weak PE brush compression by substituting D by $\Delta D + 2\xi_h$ in eq 42,

$$\sigma_{brush} = \eta_s \frac{V}{\Delta D + 2\xi_h} \quad (44)$$

with effective viscosity

$$\eta_{eff} = \sigma_{brush}\frac{D}{V} \approx \eta_s \frac{D}{\Delta D + 2\xi_h} \quad (45)$$

enhanced with respect to the solvent viscosity η_s by the geometric factor $D/(\Delta D + 2\xi_h)$. If the thickness H_0 of the PE brush is much smaller than spacing between grafted surfaces $H_0 \ll D$, the shear stress

$$\sigma_{brush} = \eta_s \frac{V}{D - 2H_0 + 2\xi_h} \simeq \eta_s \frac{V}{D}, \quad \text{for } D \gg H_0 \quad (46)$$

is similar to the shear stress between two bare charged surfaces (eq 42). The effective viscosity η_{eff} (eq 45) in this regime of weak PE brush compression is approximately equal to the solvent viscosity η_s. The reduced viscosity

$$\eta_{eff}/\eta_s \simeq 1, \quad \text{for } D > H_0$$

is close to unity, as depicted in Figure 3 by the plateau located at distances between surfaces $D > H_0$.

3.2.2. Regime of Intermediate Compression ($L < D < H_0$). As the distance between grafted surfaces approaches the thickness of uncompressed brushes $D \approx H_0$, the size of the gap $D - 2H + 2\xi_h$ rapidly decreases. The corresponding shear stress (eq 44) and the effective viscosity (eq 45) increase and become much larger than in the case of the bare charged surfaces at the same spacing D (eqs 42 and 43). The reduced viscosity becomes much larger than unity $\eta_{eff}/\eta_s \gg 1$ (see Figure 3).

As the spacing between the surfaces becomes smaller than the uncompressed brush thickness $D \lesssim H_0$, the width ΔD of the polymer-free gap between apposing brushes decreases

dx.doi.org/10.1021/ma500772a | Macromolecules 2014, 47, 5825−5838

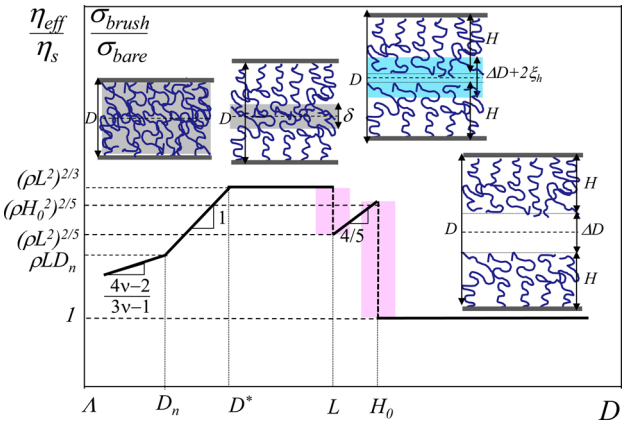

Figure 3. Reduced effective viscosity η_{eff}/η_s (equal to enhancement of shear stress $\sigma_{brush}/\sigma_{bare}$) as a function of distance D between surfaces in logarithmic coordinates. Charges on polyions and mobile ions are not shown, brush interpenetration regions are shadowed gray, the gap of laminar solvent flow with width $\Delta D + 2\xi_h$ is shadowed blue. Regions with sharp increase in reduced effective viscosity η_{eff}/η_s are shadowed pink.

below the hydrodynamic penetration length ξ_h, and the thickness of the effective gap saturates at $2\xi_h$ with

$$\xi_h \approx \frac{D^{1/5}}{\rho^{2/5}}, \quad \text{for } L < D < H_0 \tag{47}$$

estimated assuming Gaussian elasticity of polyions (see Appendix for details). In this case the shear stress due to penetration of flow inside polyelectrolyte brushes weakly increases with decreasing separation D between plates

$$\sigma_{brush} \approx \eta_s \frac{V}{\xi_h} \approx \eta_s V \frac{\rho^{2/5}}{D^{1/5}}, \quad \text{for } L < D < H_0 \tag{48}$$

and the reduced effective viscosity

$$\frac{\eta_{eff}}{\eta_s} \approx \frac{D}{\xi_h} \approx (\rho D^2)^{2/5}, \quad \text{for } L < D < H_0 \tag{49}$$

is much larger than unity and decreases with decreasing D (see Figure 3). The sharp increase of the effective viscosity at plates separation $D \approx H_0$ is by the large factor $(\rho H_0^2)^{2/5}$. Note that although the effective viscosity is much higher than the solvent viscosity, the actual viscosity in the lubrication layer is still solvent-like η_s because the concentration of polymer segments in this layer is small.

3.2.3. Regime of Strong Compression ($D < L$). The solvent-like friction is replaced with the polymer solution-type friction at the boundary between intermediate and strong compression regimes $D \simeq L$. This corresponds to another sharp increase of shear stress and effective viscosity upon compression (see the vertical dashed line at $H = L$ in Figure 3). The concentration of polymer segments $c = 2N\rho/D$ in the regime of strong compression $D \ll L$, becomes almost uniform in the gap between the grafted surfaces.

Subregime of Partially Penetrating PE Chains ($D_* < D < L$). In this subregime, the lateral force σ_{brush} is governed by the polymer solution - type friction in the interpenetration zone with thickness δ. Polymer segments from one brush in this zone are dragged with velocity $\sim V$ with respect to segments from the apposing brush. Assuming that hydrodynamic interactions are screened on length scales on the order of correlation length ξ and that the chains are unentangled, the friction force per correlation blob of size ξ can be estimated by the Stocks law as $V\eta_s\xi$. Therefore, the total shear stress is given by

$$\sigma_{brush} \simeq V\eta_s\xi n_B \simeq V\eta_s\delta/\xi^2 \tag{50}$$

where $n_B \approx \delta/\xi^3$ is the number of correlation blobs per unit area in the interpenetration zone. The interpenetration length δ for partially interpenetrating PE brushes can be estimated using eq 34

$$\delta \simeq (bN/\rho)^{1/3}(u^2 f)^{(1-\nu)/(6-3\nu)} \simeq (L/\rho)^{1/3} \tag{51}$$

and is compression-independent and does not depend on distance D between plates in the interval of $D^* < D < L$. The resulting friction stress

$$\sigma_{brush} \simeq V\eta_s b^{4/3}\rho^{-1/3}N^{1/3}(u^2 f)^{4(1-\nu)/(6-3\nu)}c \simeq \eta_{eff}(V/D) \tag{52}$$

increases linearly with concentration $c = 2N\rho/D$ or reciprocally with spacing D between grafted surfaces upon PE brush compression ($\sigma \sim c \sim D^{-1}$). Therefore, the reduced effective viscosity

$$\eta_{eff}/\eta_s \simeq (\rho b^2)^{2/3}N^{4/3}(u^2 f)^{4(1-\nu)/(6-3\nu)} \simeq (\rho L^2)^{2/3} \tag{53}$$

is independent of the distance between grafted surfaces D in this strong compression regime with partially interpenetrating PE brushes. This behavior of reduced effective viscosity η_{eff}/η_s is depicted by the high plateau located to the left of the dashed vertical lines in Figure 3. The jump of the effective viscosity at $D \approx L$ is by the factor $(\rho L^2)^{4/15}$.

This regime of constant reduced effective viscosity η_{eff}/η_s ends at the separation between grafted surfaces D on the order of the compression-independent interpenetration length δ (eq 51)

$$D_* \simeq \left(\frac{bN}{\rho}\right)^{1/3}(u^2 f)^{(1-\nu)/(6-3\nu)} \simeq \left(\frac{L}{\rho}\right)^{1/3} \simeq \delta \tag{54}$$

Note that at this boundary of the subregime the plate separation D_* (eq 54) is on the order of the fluctuations of the polyelectrolyte chains R (eq 33)—the size of unstretched chains, as expected for the interpenetration zone.

Subregime of Fully Penetrating PE Chains ($D < D_*$). At smaller separations between grafted surfaces, $D < R$, there is full interpenetration between chains from apposing brushes and all D/ξ^3 correlation blobs per unit area contribute to the friction force. The resulting friction stress in this regime

$$\sigma_{brush} \simeq \frac{V\eta_s D}{\xi^2} \simeq V\eta_s b\rho N(u^2 f)^{(1-\nu)/(2-\nu)} \tag{55}$$

is D-independent. The corresponding effective viscosity $\eta_{eff} = \sigma D/V$ is proportional to the separation D between grafted surfaces. This behavior of the reduced viscosity

$$\eta_{eff}/\eta_s \simeq bD\rho N(u^2 f)^{(1-\nu)/(2-\nu)} \simeq \rho DL \tag{56}$$

is depicted by the solid line with slope 1 in Figure 3.

Subregime of Quasi-Neutral Chains. At very strong compressions with $D < D_n$ (eq 36) the correlation length ξ of the space between plates is governed by the nonelectrostatic interactions (eq 37), and the friction stress σ approaches the value for neutral brushes[8]

dx.doi.org/10.1021/ma500772a | Macromolecules 2014, 47, 5825−5838

$$\sigma_{brush} \simeq \frac{V\eta_s D}{\xi^2} \simeq V\eta_s N\rho b\left(\frac{N\rho b^3}{D}\right)^{(1-\nu)/(3\nu-1)} \quad (57)$$

with the effective viscosity

$$\eta_{eff} = \frac{\sigma D}{V} \simeq \eta_s\left(\frac{D}{\xi}\right)^2 \sim \eta_s\left(\frac{D}{b}\right)^2\left(\frac{N\rho b^3}{D}\right)^{2\nu/(3\nu-1)} \quad (58)$$

This effective viscosity is independent of distance D between grafted surfaces for a brush in Θ-solvent with $\nu = 1/2$. In good solvent with $\nu = 3/5$ the effective viscosity in quasi-neutral regime decreases as square root of plate separation D. The reduced viscosity η_{eff}/η_s in this quasi-neutral regime is indicated by the line with slope $(4\nu-2)/(3\nu-1)$ in the left part of Figure 3.

4. DISCUSSION

4.1. Bare Charged Surfaces vs PE Brushes. Comparison of forces between bare charged and polyelectrolyte-decorated surfaces with the same surface charge density (eqs 42, 44, 52, and 55) indicates that polyelectrolyte brushes considerably enhance both normal and lateral forces at distances smaller than original brush thickness $D \lesssim H_0$. This enhancement for planar substrates decorated with PE brushes with respect to bare plates with equivalent surface charge density $ef N\rho$ is demonstrated in Figure 3 displaying the ratio of lateral (friction) stresses $\sigma_{brush}/\sigma_{bare} = \eta_{eff}/\eta_s$ and in Figure 4 presenting the ratio of normal pressures P_{brush}/P_{bare} as functions of the separation between plates D.[37]

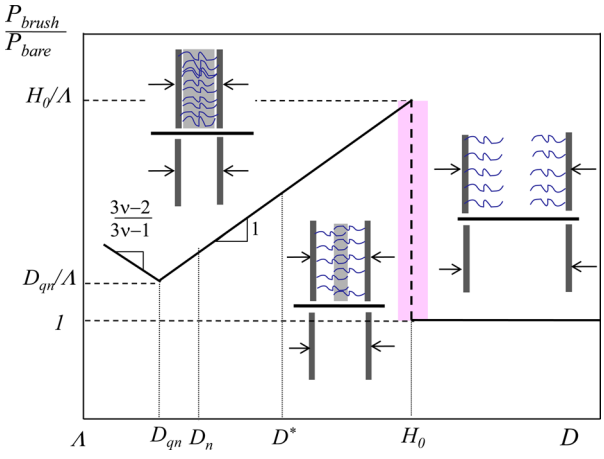

Figure 4. Ratio of normal forces per unit area P_{brush}/P_{bare} for PE brush-decorated and bare surfaces with the same surface charge density as a function of distance D in logarithmic coordinates. Region of sharp increase in P_{brush}/P_{bare} is shadowed pink.

Comparison of Normal Stresses. The enhancement of normal force per unit area P is very large: the ratio is

$$P_{brush}/P_{bare} \simeq D/\Lambda, \quad \text{for } D_{qn} < D \lesssim H_0 \quad (59)$$

with the largest value on the order of H_0/Λ at plate separation $D \approx H_0$. The ratio of normal stresses P_{brush}/P_{bare} remains much larger than unity in the whole interval of compressions $D < H_0$ passing through a minimum at distance between plates $D \simeq D_{qn}$, as shown in Figure 4. The physical reason for this large enhancement of pressure (eq 59) is the difference between the counterion distributions in the two cases. Counterions are localized within the volume of the polyelectrolyte brush and the pressure P_{brush} quickly increases upon compression of the PE brush down to $D \simeq H_0$. In the case of bare charged surfaces, counterions are localized very close to the surfaces with half of them within the Gouy−Chapman layer of thickness Λ much smaller than the brush thickness $\Lambda \ll H_0$. Therefore, the normal stress P_{bare} between bare surfaces is due to the confinement of loose tails of ion distributions (eq 40) at distances $\Lambda < D < H_0$, and is very small because counterion concentration is very low outside the Gouy−Chapman layer. At separations between plates smaller than D_{qn} at which polyelectrolyte brushes exhibit quasi-neutral behavior (eq 39), the ratio of normal forces is

$$\frac{P_{brush}}{P_{bare}} \simeq (N\rho b^2)^{3\nu/(3\nu-1)} u\left(\frac{D}{b}\right)^{(3\nu-2)/(3\nu-1)}, \quad \text{for } D \lesssim D_{qn} \quad (60)$$

with exponent $-(2-3\nu)/(3\nu-1)$ (see Figure 4) equal to -1 in Θ solvents and $-1/4$ in good solvents.

Comparison of Friction Stresses. Friction forces between polymer-decorated surfaces are also considerably enhanced compared to these for bare surfaces (see Figure 3). The distribution of counterions is not as important because counterions do not directly participate in friction. The first sharp increase of shear stress upon compression of brushes

$$\sigma_{brush}/\sigma_{bare} \simeq \eta_{eff}/\eta_s \simeq (\rho H_0^2)^{2/5}, \quad \text{for } D \simeq H_0 \quad (61)$$

is due to the reduction of the thickness of lubrication layer from H_0 to ξ_h at plate separations $D \approx H_0$. The enhancement of shear stress in the intermediate compression regime is (see eq 49)

$$\sigma_{brush}/\sigma_{bare} \simeq \eta_{eff}/\eta_s \simeq (\rho D^2)^{2/5}, \quad \text{for } L < D < H_0 \quad (62)$$

The second sharp increase of shear stress by the factor $(\rho L^2)^{4/15}$ at plate separations $D \simeq L$, occurs because solvent-like friction is substituted by polymer solution-type friction in the interpenetration zone between apposing brushes. The high ratio of friction stresses (eq 53)

$$\sigma_{brush}/\sigma_{bare} \simeq \eta_{eff}/\eta_s \simeq (\rho L^2)^{2/3}, \quad \text{for } D_* < D < L \quad (63)$$

is independent of plate separation D in the first regime of strong compression because interpenetration length δ is D-independent in this regime (see plateau in Figure 3).

In the second regime of strong compression with full interpenetration of apposing brushes the ratio of friction stresses (eq 56)

$$\sigma_{brush}/\sigma_{bare} \simeq \eta_{eff}/\eta_s \simeq \rho DL, \quad \text{for } D_n < D < D_* \quad (64)$$

decreases linearly with distance between plates D (see eq 56). Note that enhancement of friction stresses between grafted surfaces $\sigma_{brush}/\sigma_{bare}$ in all regimes with $D < H_0$ is smaller than the ratio of normal forces P_{brush}/P_{bare}. This explains why polymer brushes are better lubricants than simple liquids as discussed in detail below.

4.2. Friction Coefficient. Friction coefficient is conventionally defined[1] as the ratio of friction to normal forces

$$\mu = \sigma/P \quad (65)$$

The normal force−pressure P between apposing brushes is velocity-independent in the linear regime, while the shear stress

dx.doi.org/10.1021/ma500772a | Macromolecules 2014, 47, 5825−5838

σ is linearly proportional to sliding velocity V. Therefore, friction coefficient μ for brushes is a velocity-dependent quantity, and thus does not directly characterize the properties of participating surfaces unlike the friction coefficient between solid surfaces. In particular, one can always select small enough velocity to obtain as low friction coefficient μ as one would like. Note that the friction coefficient μ_{bare} between bare charged surfaces is also velocity-dependent

$$\mu_{bare} \simeq \eta_s V \frac{l_B D}{k_B T}, \quad \text{for } D > > \Lambda \tag{66}$$

where we used eqs 40, 42, and 65, while the case $D < \Lambda$ is not of practical interest for strongly charged surfaces with $\Lambda \lesssim b$.

Nevertheless the velocity-dependent friction coefficients μ can be compared between different pairs of surfaces at similar shear conditions. By using the results of previous subsections, we compare friction coefficients for two systems: planar surfaces decorated by osmotic polyelectrolyte brushes and bare charged surfaces with equivalent charge density

$$\frac{\mu_{brush}}{\mu_{bare}} = \frac{\sigma_{brush}}{\sigma_{bare}} \frac{P_{bare}}{P_{brush}} \tag{67}$$

For polyelectrolyte-decorated surfaces at large distances $D \gg H_0$ between plates, the friction coefficient (calculated with eqs 27 and 46)

$$\mu_{brush} \simeq \eta_s V \frac{l_B D}{k_B T}, \quad \text{for } D \gg H_0 \tag{68}$$

is almost unaffected by the presence of polymer brushes. This behavior of μ is indicated in Figure 5a by solid line with slope 1 at large separations $D \gg H_0$ between plates and is the same as between bare surfaces (eq 66).

$$\mu_{brush}/\mu_{bare} \approx 1, \quad \text{for } D \gg H_0$$

(see the corresponding horizontal line in Figure 5b).

At the boundary between weak and intermediate compressions ($D \approx H_0$) both the normal and shear stresses sharply increase, but the friction coefficient μ_{brush} drops because enhancement of normal force by factor H_0/Λ is stronger than enhancement of friction stress between the brush-decorated surfaces by factor $(\rho H_0^2)^{2/5}$at relatively high grafting densities of polyions in the osmotic regime with $\rho/\rho_{osm} > (uf^\nu)^{-2/3} > 1$. This case is depicted in Figure 5b.

In the regime of intermediate compression, $L < D < H_0$, the friction stress σ_{brush} is still solvent-like, but is enhanced in comparison to shear stress between bare charged surfaces due to very thin lubrication layer between brushes. In this regime of intermediate compression the thickness ΔD of the gap between brushes is already much smaller than the hydrodynamic penetration length ξ_h. The latter determines the effective gap thickness where the friction remains solvent-like. The normal pressure P_{brush} between brushes is enhanced more than shear stress σ_{brush} due to the contribution to the pressure from almost all counterions. In this interval of distances D, the friction coefficient μ_{brush} is estimated assuming Gaussian elasticity of polyions (using eqs 28 and 48) as

$$\mu_{brush} = \frac{\sigma_{brush}}{P_{brush}} \simeq \eta_s V \frac{D^{4/5}}{k_B T N f \rho^{3/5}}, \quad \text{for } L < D < H_0 \tag{69}$$

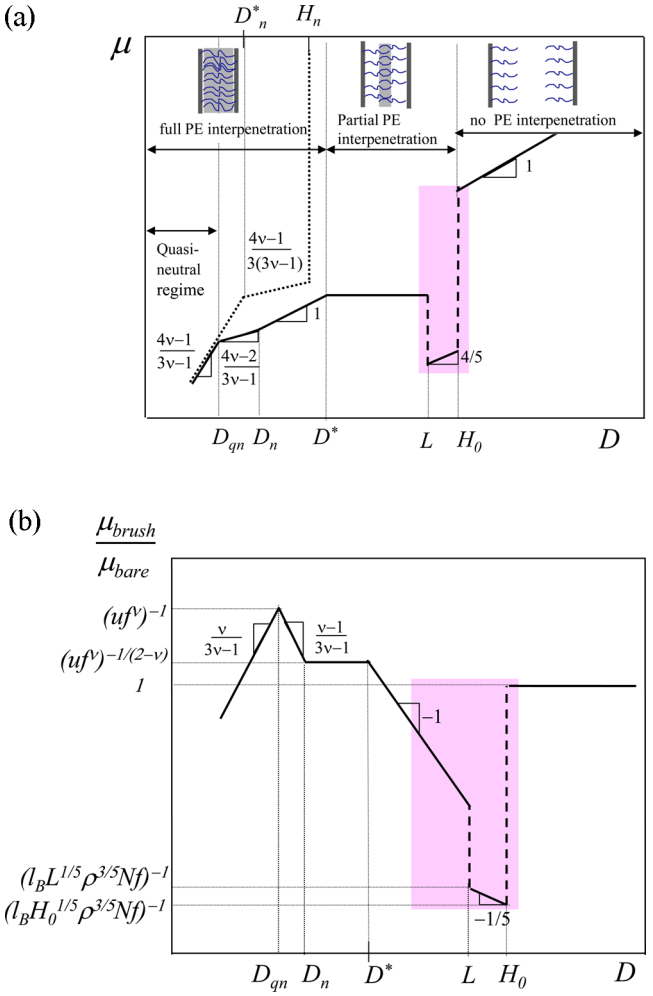

Figure 5. (a) Friction coefficient μ between planar surfaces decorated by PE brushes (solid lines) and neutral brushes with the same degree of chain polymerization N and grafting density ρ (dotted lines) as a function of distance D between surfaces in logarithmic coordinates. (b) Ratio of friction coefficients μ_{brush}/μ_{bare} for PE brush-decorated and bare surfaces with the same surface charge density in logarithmic coordinates. The region of enhanced lubrication by PE brushes is shadowed pink.

decreasing as $\mu_{brush} \sim D^{4/5}$ upon the decrease in plate separation D (see line with slope 4/5 in Figure 5a). The ratio of friction coefficients

$$\frac{\mu_{brush}}{\mu_{bare}} \approx \frac{1}{l_B D^{1/5} \rho^{3/5}}, \quad \text{for } L < D < H_0 \tag{70}$$

drops sharply at $D \simeq H_0$ and weakly increases as $\mu_{brush}/\mu_{bare} \sim D^{-1/5}$ with decreasing D (see Figure 5b).

The sharp increase of the friction coefficient μ_{brush} at $D \simeq L$ indicated by the left vertical dashed line in Figure 5a is associated with the interpenetration of PE chains and the appearance of polymer solution-type friction. PE brushes start to overlap in the regime of strong compressions at distances between plates $D < L$ and the friction coefficient (calculated using eqs 28 and 52)

$$\mu_{brush} = \frac{\sigma_{brush}}{P_{brush}} \simeq \eta_s V \frac{(\rho L^2)^{2/3}}{k_B T f N \rho}, \quad \text{for } D_* < D < L \tag{71}$$

dx.doi.org/10.1021/ma500772a | Macromolecules 2014, 47, 5825−5838

Table 1. [a] Normal Pressure $P_{brush}/(k_BT)$, Reduced Effective Viscosity η_{eff}/η_s, and Ratio of Friction Coefficients μ_{brush}/μ_{bare} between a Pair of Apposing Polyelectrolyte Brushes with Weakly Charged Chains $bf^{-\nu} < l_B$

regimes	$P_{brush}/(k_BT)$	$\eta_{eff}/\eta_s = \sigma_{brush}/\sigma_{bare}$	μ_{brush}/μ_{bare}
$D \gg H_0$	$(l_BD^2)^{-1}$	1	1
$L < D < H_0$	$fN\rho/D$	$(\rho D^2)^{2/5}$	$(l_BD^{1/5}\rho^{3/5})^{-1}$
$D_* < D < L$	$fN\rho/D$	$(\rho L^2)^{2/3}$	$(\rho L^2)^{2/3}/(f\ N\ l_B\rho D)$
$D_n < D < D_*$	$fN\rho/D$	ρDL	$(uf^\nu)^{-1/(2-\nu)}$
$D_{qn} < D < D_n$	$fN\rho/D$	$(N\rho b^3/D)^{2\nu/(3\nu-1)}\ (D/b)^2$	$(1/uf)(N\rho b^3/D)^{(1-\nu)/(3\nu-1)}$
$D < D_{qn}$	$b^{-3}(N\rho b^3/D)^{3\nu/(3\nu-1)}$	$(N\rho b^3/D)^{2\nu/(3\nu-1)}\ (D/b)^2$	$(1/u)[D/(N\rho b^3)]^{\nu/(3\nu-1)}$

[a] Here $\sigma_{bare} \approx \eta_s V/D$ and $\mu_{bare} \approx \eta_s V l_B D/k_BT$ are shear stress and friction coefficient between bare surfaces with the same charge density $e\,f\,N\,\rho$ as polyelectrolyte brushes.

is independent of the distance D between plates. This behavior of μ_{brush} is shown by the horizontal line in Figure 5a. The ratio of friction coefficients in this regime

$$\frac{\mu_{brush}}{\mu_{bare}} \approx \frac{(\rho L^2)^{2/3}}{fNl_B\rho D}, \quad \text{for } D_* < D < L \tag{72}$$

varies reciprocally with spacing between plates D ($\mu_{brush}/\mu_{bare} \sim D^{-1}$, see the line with slope −1 in Figure 5b).

As polyelectrolyte brushes fully interpenetrate each other at distances $D_n < D < D_*$, eqs 28 and 55 give friction coefficient

$$\mu = \eta_s V \frac{DL}{k_BTfN}, \quad \text{for } D_n < D < D_* \tag{73}$$

linearly proportional to plate separation (as indicated by the solid line with slope 1 at $D < D_*$ in Figure 5a). The ratio of friction coefficients

$$\frac{\mu_{brush}}{\mu_{bare}} \approx \frac{L}{fNl_B} \approx (uf^\nu)^{-1/(2-\nu)}, \quad \text{for } D_n < D < D_* \tag{74}$$

is independent of plate spacing D (left horizontal line in Figure 5b). Note that $uf^\nu < 1$ for charge density f below Manning condensation threshold[33] and $uf_{eff}^\nu = 1$ for highly charged chains with f above this threshold. Therefore, the ratio of friction coefficients in this regime is greater than or on the order of unity, indicating that polyelectrolyte brushes can produce solvent-like friction at very high normal loads.

At larger compressions $D_{qn} < D < D_n$, correlation length ξ is governed by nonelectrostatic interactions (eq 37) while the normal pressure is still determined by mobile counterions. By using eqs 28 and 57 one finds friction coefficient in this mixed subregime,

$$\mu_{brush} \simeq \eta_s V \frac{N\rho b^4}{k_BTf}\left(\frac{D}{N\rho b^3}\right)^{2(2\nu-1)/(3\nu-1)}, \quad \text{for } D_{qn} < D < D_n \tag{75}$$

with no D-dependence in Θ-solvent ($\nu = 1/2$) and decreasing as $\mu \sim D^{1/2}$ upon further compression under good solvent conditions ($\nu = 3/5$). Scaling dependence for μ in this subregime is shown in Figure 5a by the solid line with exponent $(4\nu - 2)/(3\nu - 1)$. The corresponding ratio of friction coefficients in this mixed regime

$$\frac{\mu_{brush}}{\mu_{bare}} \simeq \frac{1}{uf}\left(\frac{N\rho b^3}{D}\right)^{(1-\nu)/(3\nu-1)}, \quad \text{for } D_{qn} < D < D_n \tag{76}$$

increases with decreasing D as indicated by the line with slope $(\nu - 1)/(3\nu - 1)$ in Figure 5b.

Finally the compressed polyelectrolyte brushes behave as quasi-neutral at distances between plates $D < D_{qn}$. The friction coefficient in this subregime is determined by eqs 39 and 57 as

$$\mu_{brush} \simeq \frac{V\eta_s D\xi}{k_BT} \simeq \eta_s V \frac{N\rho b^4}{k_BT}\left(\frac{D}{N\rho b^3}\right)^{(4\nu-1)/(3\nu-1)}, \quad \text{for } D < D_{qn} \tag{77}$$

and decreases upon compression as sketched in Figure 5a by the solid line with exponent $(4\nu - 1)/(3\nu - 1)$. In Θ solvent with $\nu = 1/2$, this exponent is equal to 2 while in good solvent with $\nu = 3/5$ it decreases to 7/4. The ratio of friction coefficients between a pair of quasi-neutral brushes μ_{brush} and a pair of bare charged surfaces μ_{bare}

$$\frac{\mu_{brush}}{\mu_{bare}} \simeq \frac{1}{u}\left(\frac{D}{N\rho b^3}\right)^{\nu/(3\nu-1)} \simeq u^{-1}(cb^3)^{-\nu/(3\nu-1)}, \quad \text{for } D < D_{qn} \tag{78}$$

decreases with decreasing D, as indicated by the line with slope $\nu/(3\nu - 1)$ in Figure 5b and can become less than unity at high enough compression as long as polymer volume fraction between plates is still low.

As shown in Figure 5b, the brush-decorated surfaces can produce noticeably smaller friction coefficient compared to friction between bare charged surfaces. A significant drop in μ_{brush}/μ_{bare} is achieved for polyelectrolyte brushes in the interval of distances between plates $D_* < D < H_0$. This range of conditions is marked by shadowed (pink) region in Figure 5b. Here, charged polymer brushes behave as better lubricants than low molecular weight liquids, while supporting much higher loads. Different regimes of friction between polyelectrolyte brushes are summarized in Table 1.

Note that the volume fraction of monomers $cb^3 \approx N\rho b^3/D$ in the compressed brushes is assumed to be much less than unity in all regimes to avoid the effect of high monomeric friction coefficient and glass transition of bulk polymers.

The schematic behavior of the friction coefficient μ for neutral polymer brushes (with fraction of charged monomers $f = 0$) and the same grafting density ρ is depicted by the dotted lines in Figure 5a. In contrast to polyelectrolyte brushes, neutral polymer brushes start to interact with each other at distances $D \simeq H_n$ with unperturbed brush thickness H_n specified by eq 20 (indicated by the dotted vertical line in Figure 5a). At stronger compressions, $D_n^* < D < H_n$ (with distance D_n^* on the order of unperturbed chain length in semidilute polymer solution with concentration $N\rho/D_n^*$), neutral brushes are partially inter-

dx.doi.org/10.1021/ma500772a | Macromolecules 2014, 47, 5825−5838

Table 2. Normal Pressure $P_{brush}/(k_BT)$, Reduced Effective Viscosity η_{eff}/η_s, and Ratio of Friction Coefficients μ_{brush}/μ_{bare} between a Pair of Apposing Polyelectrolyte Brushes with Strongly Charged ($bf^{-\nu} > l_B$) Flexible ($b < l_B$) Chains[a]

regimes	$P_{brush}/(k_BT)$	$\eta_{eff}/\eta_s = \sigma_{brush}/\sigma_{bare}$	μ_{brush}/μ_{bare}
$D \gg H_0 \simeq L$	$(l_BD^2)^{-1}$	1	1
$D_* < D < L$	$u^{-1/\nu}N\rho/D$	$\rho^{2/3}(bNu^{(\nu-1)/\nu})^{4/3}$	$b^{1/3}N^{1/3}u^{(\nu-1)/3\nu}/(\rho^{1/3}D)$
$D_n < D < D_*$	$u^{-1/\nu}N\rho/D$	$\rho DbNu^{(\nu-1)/\nu}$	1
$D < D_{qn} \simeq D_n$	$b^{-3}(N\rho b^3/D)^{3\nu/(3\nu-1)}$	$(N\rho b^3/D)^{2\nu/(3\nu-1)}\ (D/b)^2$	$(1/u)[D/(N\rho b^3)]^{\nu/(3\nu-1)}$

[a]Here $\sigma_{bare} \approx \eta_s V/D$, $\mu_{bare} \approx \eta_s V l_B D/k_BT$ are shear stress and friction coefficient between bare surfaces with the same charge density $efN\rho$ as polyelectrolyte brushes.

penetrating, and the decrease in friction coefficient μ in this subregime is indicated by the dotted line with slope $(4\nu - 1)/[3(3\nu - 1)]$ (that is, 7/12 for $\nu = 3/5$, and 2/3 for $\nu = 1/2$). In the regime of full interpenetration of neutral brushes at distances $D < D_n^*$, friction coefficient μ is described by eq 77 and is depicted by the dotted line with slope $(4\nu - 1)/(3\nu - 1)$ (that is, 7/4 for $\nu = 3/5$, and 2 for $\nu = 1/2$) in Figure 5a. As shown in Figure 5a, polyelectrolyte brushes provide lower friction coefficient than neutral brushes at the same conditions (same sliding velocity, mass per unit area, and plate separation) except for very strong compressions with distance between plates $D < D_{qn}$ at which polyelectrolyte brushes exhibit quasi-neutral behavior and friction coefficients of polyelectrolyte and neutral brushes are similar.

Our theoretical predictions were obtained for salt-free solutions, but they are also applicable for solutions with added salt as long as salt concentration c_s is lower than the concentration of counterions, $c_i = 2fN\rho/D$. The concentration of counterions c_i in the gap between apposing brushes increases upon compression (with the decrease of the spacing D between plates), and the applicability of our results expands at stronger compressions.

4.3. Effect of Counterion Condensation on Friction between Polyelectrolyte Brushes. The equations discussed above and summarized in Table 1 were derived for flexible weakly charged polyelectrolytes with degree of ionization below the Manning condensation threshold ($bf^{-\nu} < l_B$, where f is the number of elementary charges per Kuhn length b). If the charge density f, increases up to the value of $f \approx u^{-1/\nu}$ both the size of electrostatic blob (ξ_e), and the distance between charges along the chain (L/fN) approach the value of the Bjerrum length (l_B). At higher bare charge densities $f > u^{-1/\nu}$ the Manning condensation of counterions maintains the distance l_B between the uncondensed charges along the polyion with the effective charge density $f_{eff} \approx u^{-1/\nu}$. There is no Pincus regime with intermolecularly induced stretching for such strongly charged brushes with condensed counterions because $\rho_{osm} \approx \rho^* \approx L^{-2}$ (see eqs 11 and 16). In this counterion condensation regime with $f_{eff} \approx u^{-1/\nu}$, brush height $H \approx H_0 \approx L \simeq bNu^{(\nu-1)/\nu}$ is independent of chain grafting density ρ (eq 17 and 3).

For these brushes with condensed counterions the regime of intermediate compression with interval of distances $L < D < H_0$ between surfaces shrinks into the crossover region between the regime of weak compression (with $D \gg H_0 \simeq L$) and the regime of strong compression (with $D < L$). There is also no mixed subregime with interval of distances between surfaces $D_{qn} < D < D_n$. The two remaining crossover distances separating various subregimes in the regime of strong brush compression (eqs 54, 36, and 38) are $D_* \simeq (bNu^{[(2\nu-1)(1-\nu)]/[\nu(2-\nu)]}/\rho)^{1/3}$ and $D_n \simeq D_{qn} \simeq b^3N\rho u^{(3\nu-1)/\nu}$. By substituting the effective charge density $f_{eff} \approx u^{-1/\nu}$ and $L \simeq Nbu^{(\nu-1)/\nu}$ into the corresponding equations for shear stress σ_{brush} and the friction coefficient μ, one finds the reduced effective viscosity η_{eff}/η_s and the ratio of friction coefficients μ_{brush}/μ_{bare} for strongly charged ($f > u^{-1/\nu}$) flexible polyions with electrostatic interaction parameter $u = l_B/b > 1$ (see Table 2).

In the case of stiff chains with $b > l_B$ there is another regime with increasing charge density f preceding counterion condensation regime. If charge density f is higher than $u^{-1/2}$ the electrostatic blob size ξ_e becomes smaller than Kuhn length b. These stiff polyelectrolyte chains are almost fully stretched with end-to-end distance approaching contour length bN but for $u^{-1/2} < f < u^{-1}$ there is no counterion condensation. At higher charge densities $f > u^{-1}$ counterions condense on these almost fully stretched polyions saturating the effective charge density at the Manning value of one charge per Bjerrum length corresponding to effective charge density $f \approx 1/u$ charges per Kuhn length.

For flexible polyelectrolytes with a typical Kuhn segment length $b \simeq 1.5-2.0$ nm, the value of electrostatic parameter $u = l_B/b$ is estimated in water to be $u \simeq 0.3-0.5$. That is, in scaling terms $u = l_B/b$ is close to unity, and many experimental systems (e.g., ref 13) are at the crossover between the scaling regimes with $u \gg 1$ and $u \ll 1$. For strongly charged polyelectrolytes with condensed counterions, one can approximate this crossover region by substituting $u = 1$ in the equations presented in this subsection to find brush thickness $H_0 \simeq L \simeq bN$, and two threshold spacings between surfaces $D_* \simeq (bN/\rho)^{1/3}$ and $D_n \simeq D_{qn} \simeq b^3N\rho$. The subregime of quasi-neutral brush behavior is shifted to very high polymer concentrations $b^3N\rho/D_n \simeq 1$ in the gap between surfaces, and is thereby eliminated. By substituting $u = 1$ in Table 2 above we find the reduced effective viscosity η_{eff}/η_s and relative friction coefficient μ_{brush}/μ_{bare} for the case of crossover electrostatic parameter $u = l_B/b \simeq 1$ (Table 3).

Table 3. [a] Normal Pressure $P_{brush}/(k_BT)$, Reduced Effective Viscosity η_{eff}/η_s, and Ratio of Friction Coefficients μ_{brush}/μ_{bare} between a Pair of Apposing Strongly Charged ($bf^{-\nu} > l_B$) Polyelectrolyte Brushes with $l_B = b$

regimes	$P_{brush}/(k_BT)$	$\eta_{eff}/\eta_s = \sigma_{brush}/\sigma_{bare}$	μ_{brush}/μ_{bare}
$D \gg bN$	$(l_BD^2)^{-1}$	1	1
$D_* < D < bN$	$N\rho/D$	$\rho^{2/3}(bN)^{4/3}$	$D_*/D < 1$
$D < D_*$	$N\rho/D$	ρDbN	1

[a]Here the crossover plate separation $D_* \simeq (bN/\rho)^{1/3}$.

At separations D between surfaces much larger than brush thickness bN, effective viscosities, shear stresses, and friction coefficients between pairs of apposing brushes and between pairs of bare surfaces are almost the same (all ratios are ≈1). Upon intermediate compression with partial interpenetration between brushes ($D_* < D < bN$) the enhancement of shear

dx.doi.org/10.1021/ma500772a | Macromolecules 2014, 47, 5825−5838

stress $\sigma_{brush}/\sigma_{bare}$ is smaller than the enhancement of normal stress P_{brush}/P_{bare} and the relative friction coefficient between brushes μ_{brush} is smaller than friction coefficient between bare surfaces μ_{bare} by the factor $\mu_{brush}/\mu_{bare} \approx D_*/D$. Upon further compression ($D < D_*$) friction coefficients between polyelectrolyte brushes and bare surfaces are the same, but brushes support much higher load.

5. CONCLUSIONS

The scaling theory developed in this paper is applicable for brushes with relatively short polyelectrolyte chains with no entanglements at salt-free conditions and for low sliding velocities V (linear response regime with friction stress σ proportional to shear rate). In addition to the electrostatic interactions between charged species, the model accounts for the short-range two-body and three-body monomer−monomer interactions (with scaling exponents $\nu = 3/5$ and $\nu = 1/2$ for good or Θ solvent conditions, respectively). The simple scaling model neglects the higher order nonelectrostatic interactions between monomers and the changes in the dielectric constant and monomeric friction coefficient that become significant at higher polymer concentrations (i.e., at strong compressions of the brushes).

The decrease in distance D between brush-decorated surfaces gives rise to a sequence of regimes that are characterized by different scaling dependences for friction coefficient μ. The full set of regimes is predicted for grafting densities of polyions $\rho < b^{-2}N^{-1/2}$ that are not too high. For this interval of grafting densities, at the maximum compression of brushes to the polymer volume fraction between surfaces close to unity, the distance between surfaces D is smaller than the Gaussian size of the polyions. For higher grafting densities $\rho > b^{-2}N^{-1/2}$some subregimes predicted for strong compressions of brushes disappear.

We demonstrate that enhanced lubricating properties of polyelectrolyte brushes compared to bare surfaces with equivalent surface charge density are linked to confinement of mobile counterions in the volume of PE brush in the osmotic regime. Compression of apposing PE brushes with interplate distances $\Lambda < D < H_0$ leads to the increase in osmotic pressure of confined counterions, $P_{brush} \sim D^{-1}$, while bare charged surfaces experience much smaller normal force, $P_{bare} \sim D^{-2}$, due to significantly lower counterion concentration outside the Gouy−Chapman layer of thickness $\Lambda \simeq (l_B \rho f N)^{-1}$. Although shear stress σ_{brush} arising upon interpenetration of sliding PE brushes is larger than the stress σ_{bare} between bare charged surfaces, the friction coefficient $\mu = \sigma/P$ remains smaller for PE brushes due to considerably higher values of pressure $P_{brush} \gg P_{bare}$ at interplate distances $\Lambda < D < H_0$. This enhancement in lubrication is provided by polyelectrolyte brushes with grafting densities of polyions $\rho > (uf^{\nu})^{-2/3}\rho_{osm}$. In the opposite case of very low grafting densities of polyions, $\rho_{osm} < \rho < (uf^{\nu})^{-2/3}\rho_{osm}$, the friction coefficient μ between bare charged surfaces is smaller than between polyelectrolyte brushes under similar conditions (same sliding velocity V and distance $\Lambda < D < H_0$ between surfaces).

Comparison of friction coefficient $\mu = \sigma/P$ for charged and neutral polymer brushes with the same mass per unit area revealed enhanced lubrication (i.e., smaller values of μ) between PE brushes. Only at strong compressions of the tethered polyions in the interval of distances $D < D_{qn}$ (in the quasi-neutral regime, see Table 1 and Figure 5a) do the friction coefficients for the two systems become similar. Recent computer simulations,[34,35,15] confirmed smaller values of friction coefficient μ for charged brushes compared to neutral systems under similar conditions. However, the simulations mostly focused on the nonlinear regime with V-dependent width of the interpenetration zone[15] and shear stress σ described by the sublinear dependence[34] on the sliding velocity V. Therefore, a comprehensive comparison between the results of computer simulations as well as experiments and the predictions of our model is still missing. The corresponding simulations are currently under way and the results and comparison between simulations and theory will be presented in a future publication.

APPENDIX

1. Neutral Brushes

Θ Solvent Conditions. Consider a tethered layer of neutral flexible chains with $N \gg 1$ Kuhn monomers (each with size b) immersed in a Θ solvent. At grafting densities $\rho \gg (b^2N)^{-1}$, the chains stretch due to the ternary repulsive interactions between monomers, and form a brush with thickness (see eq 20 with $\nu = 1/2$)

$$H_\theta \simeq b^2 N \rho^{1/2} \simeq bN(\rho b^2)^{1/2} \tag{79}$$

Under Θ-solvent conditions, the chains are almost ideal and exhibit Gaussian statistics on all length scales, and the molecular field in the brush is parabolic.[26] This results[36] in the "classic" polymer density profile within the brush with thickness H_θ

$$c(z) = c(0)\sqrt{1 - z^2/H_\theta^2} \tag{80}$$

and the distribution function of the free ends

$$g(z) = \frac{2z}{H_\theta{}^2}, \quad \text{for } 0 < z < H_\theta \tag{81}$$

where z is the distance from the grafted surface. Because of the thermal fluctuations, the density profile has fluctuation-induced "tail" with the characteristic width $\simeq b^4N^{2/3}/H_\theta{}^{1/3}$.

A laminar flow will penetrate into such a brush down to the distance ξ_h from the brush edge $z = H_\theta$. We estimate ξ_h as the distance at which chain sections at free ends in the layer of thickness $H_\theta - \xi_h$ start to overlap with each other, i.e., give rise to mesh with size $\simeq \xi_h$. This requirement is formulated as

$$(\rho \int_{H_\theta - \xi_h}^{H_\theta} g(z)\, \mathrm{d}z)^{-1/2} \simeq \xi_h \tag{82}$$

to give

$$\xi_h \simeq \left(\frac{H_\theta}{\rho}\right)^{1/3} \simeq \frac{(Nb^2)^{1/3}}{\rho^{1/6}} \simeq \frac{R_0{}^{2/3}}{\rho^{1/6}} \tag{83}$$

where $R_0{}^2 \approx Nb^2$ are the mean square fluctuations of the chain in a Θ solvent. Therefore, the hydrodynamic penetration length ξ_h in unperturbed neutral polymer brush in a Θ solvent is on the order of the tail (fluctuation) length δ_n (eq 30) with $H = H_\theta$ (eq 79).

2. Charged Brushes

Consider polyions with charge fN on each, tethered with grafting density $\rho > \rho_{osm}$ at salt-free conditions. If polyions exhibit Gaussian elasticity on all length scales, the molecular field in the brush is parabolic. This molecular field in the charged (PB) and the osmotic brush regimes is of the electrostatic origin, and therefore electrostatic potential in the

dx.doi.org/10.1021/ma500772a | Macromolecules 2014, 47, 5825−5838

brush in these regimes is parabolic. The Poisson−Boltzmann model of polyelectrolyte brushes[19] predicts the truncated Gaussian decay of the polymer density profile,

$$c(z) = \frac{N\rho}{H_0}\frac{\Lambda}{H_0}\left[1 + \frac{(H_0/\Lambda - H/H_0)\exp(-z^2/{H_0}^2)}{\int_0^{H/H_0}\exp(-t^2)\,dt}\right] \tag{84}$$

and the distribution of the free ends

$$g(z) = \frac{z}{{H_0}^2}\frac{\Lambda}{H_0}\left[\frac{H_0}{\sqrt{H^2 - x^2}}\left(1 + \frac{(H_0/\Lambda - H/H_0)\exp(-H^2/{H_0}^2)}{\int_0^{H/H_0}\exp(-t^2)\,dt}\right) + \left(\frac{H_0}{\Lambda} - \frac{H}{H_0}\right)\exp(-z^2/{H_0}^2)\frac{\int_0^{\sqrt{H^2/H_0^2 - x^2/H_0^2}}\exp(-t^2)\,dt}{\int_0^{H/H_0}\exp(-t^2)\,dt}\right] \tag{85}$$

where z is the distance from the grafted surface, and H is the brush thickness. Equations 84 and 85 are applicable to apposing brushes with distances D between grafted surfaces providing the dominance of ionic contributions over the non-electrostatic interactions between monomers. Under these conditions, the brush thickness H is specified by the solution of equation

$$\frac{H_0}{\Lambda} = \frac{H}{H_0} + \left(\frac{H}{H_0}\right)^2(1 + \beta^2)\exp(H^2/{H_0}^2)\int_0^{H/H_0}\exp(-t^2)\,dt \tag{86}$$

with parameter β related to the width $2\Delta D = D - 2H$ of the gap between brush edges as

$$\frac{1}{\beta}\arctan\left(\frac{1}{\beta}\right) = \frac{\Delta D H}{{H_0}^2} \tag{87}$$

In the osmotic brush regime, the ratio of the characteristic brush thickness (eq 17 with $\nu = 1/2$)

$$H_0 = \sqrt{\frac{8}{3\pi^2}}\,bNf^{1/2}$$

and Gouy-Chapman length Λ (eq 15), is very large $H_0/\Lambda \gg 1$. To determine the flow penetration length ξ_h in this regime we use the same arguments as for the neutral brushes. That is, we assume that hydrodynamic interactions become screened at distance $\xi_h \ll H$ if chain sections of grafted polymers above height $H - \xi_h$ overlap and create mesh with size $\simeq \xi_h$. One then can use eq 82 (with H_θ replaced by H) to find ξ_h. At distances $x \lesssim$ H distribution function of the free ends $g(z)$ in eq 85 is dominated by the first term in square brackets and is estimated in the osmotic brush regime with $H_0/\Lambda \gg 1$ as

$$g(z) \simeq \frac{z}{(\int_0^{H/H_0}\exp(-t^2)\,dt)H_0\sqrt{H^2 - z^2}} \tag{88}$$

By substituting eq 88 into eq 82, one finds that the hydrodynamic penetration length in the apposing polyelectrolyte brushes,

$$\xi_h \simeq \frac{1}{\rho^{2/5}}\begin{cases} H_0^{1/5} & \text{for } D \gtrsim H_0 \\ D^{1/5} & \text{for } D < H_0 \end{cases} \tag{89}$$

decreases as a function of distance $D < H_0$ between surfaces as $\xi_h \sim D^{1/5}$, and saturates at larger distances $D \gtrsim H_0$.

AUTHOR INFORMATION

Corresponding Author

*(M.R.) E-mail: mr@unc.edu.

Notes

The authors declare no competing financial interest.

ACKNOWLEDGMENTS

The authors would like to acknowledge financial support from the National Science Foundation under Grants DMR-1309892, DMR-1121107, and DMR-1122483, the National Institutes of Health under 1-P01-HL108808-01A1 and the Cystic Fibrosis Foundation. E.B.Z. acknowledges partial support from the Russian Fund of Basic Research (RFBR) under Grant 11-03-00969a and from the Government of Russian Federation under Grant 074-U01.

REFERENCES

(1) Raviv, U.; Giasson, S.; Kampf, N.; Gohy, J. F.; Jerome, R.; Klein, J. *Nature* **2003**, *425*, 163.
(2) Pastorino, C.; Kreer, T.; Müller, M.; Binder, K. *Phys. Rev. E* **2007**, *76*, 026706.
(3) Schorr, P. A.; Kwan, T. C. B.; Kilbey, S. M., II; Shaqfeh, E. S. G.; Tirrell, M. *Macromolecules* **2003**, *36*, 389.
(4) Murat, M.; Grest, G. S. *Macromolecules* **1989**, *22*, 4054.
(5) Murat, M.; Grest, G. S. *Phys. Rev. Lett.* **1989**, *63*, 1074−1077.
(6) Grest, G. S. *Adv. Polym. Sci.* **1999**, *138*, 150.
(7) Neelov, I. M.; Borisov, O. V.; Binder, K. *J. Chem. Phys.* **1998**, *108*, 6973.
(8) Galushko, A.; Spirin, L.; Kreer, T.; Johner, A.; Pastorino, C.; Wittmer, J.; Baschnagel, J. *Langmuir* **2010**, *26*, 6418.
(9) Klein, J. *Annu. Rev. Mater. Sci.* **1996**, *26*, 581.
(10) Sokoloff, J. B. *J. Chem. Phys.* **2008**, *129*, 014901.
(11) Harden, J. L.; Borisov, O. V.; Cates, M. E. *Macromolecules* **1997**, *30*, 1179.
(12) Birshtein, T. M.; Zhulina, E. B. *Macromol.Chem.,Theory Simul.* **1992**, *1*, 193.
(13) Raviv, U.; Giasson, S.; Kampf, N.; Gohy, J. F.; Jerome, R.; Klein, J. *Langmuir* **2008**, *24*, 8678.
(14) Liberelle, B.; Giasson, S. *Langmuir* **2008**, *24*, 1550.
(15) Ou, Y.; Sokoloff, J. B.; Stevens, M. J. *Phys. Rev. E* **2012**, *85*, 011801.
(16) Alexander, S. *J. Phys. (Paris)* **1977**, *38*, 983.
(17) de Gennes, P. G. *Macromolecules* **1980**, *13*, 1069.
(18) Miklavic, S. J.; Marčelja, S. *J. Phys. Chem.* **1988**, *92*, 6718−6722.
(19) Zhulina, E. B.; Borisov, O. V. *J. Chem. Phys.* **1997**, *107*, 5952.
(20) Israelachvili, J. *Intermolecular and Surface Forces*; Academic Press: London, 1992.
(21) Hehmeyer, O. J.; Stevens, M. J. *J. Chem. Phys.* **2005**, *122*, 134909.
(22) Pincus, P. *Macromolecules* **1991**, *24*, 2912−2919.
(23) Borisov, O. V.; Birshtein, T. M.; Zhulina, E. B. *J. Phys. II* **1991**, *1*, 521−526.
(24) Pincus, P. *Macromolecules* **1976**, *9*, 386.
(25) Rubinstein, M.; Colby, R. H. *Polymer Physics*; Oxford University Press: Oxford, U.K., 2003.
(26) Semenov, A. N. *Sov. Phys. JETP* **1985**, *61*, 733.
(27) Milner, S. T.; Witten, T. A.; Cates, M. *Macromolecules* **1988**, *21*, 2610.
(28) Skvortsov, A. M.; Pavlushkov, I. V.; Gorbunov, A. A.; Zhulina, Y. B.; Priamistsyn, V. A.; Borisov, O. V. *Vysokomol. Soedin.* **1988**, *A30*, 1615.
(29) Zhulina, E. B.; Semenov, A. N. *Polym. Sci. USSR* **1989**, *A31*, 196.
(30) Witten, T.; Leibler, L.; Pincus, P. *Macromolecules* **1990**, *23*, 824.
(31) de Gennes, P. G.; Picus, P.; Velasco, R. M.; Brochard, F. *J. Phys. (Paris)* **1976**, *37*, 1461.
(32) Dobrynin, A. V.; Rubinstein, M. *Prog. Polym. Sci.* **2005**, *30*, 1049.

(33) Zappone, B.; Ruth, M.; Greene, G. W.; Jay, G. D.; Israelachvili, J. N. *Biophys. J.* **2007**, *92*, 1693.
(34) Spirin, L.; Kreer, T. *ACS Macro Lett.* **2013**, *2*, 63−66.
(35) Goujon, F.; Ghoufi, A.; Malfreyt, P.; Tildesley, D. *Soft Matter* **2013**, *9*, 2966.
(36) Zhulina, E. B.; Borisov, O. V.; Priamitsyn, V. A.; Birshtein, T. M. *Macromolecules* **1991**, *24*, 140.
(37) Note that this high charge density is often impractical as separation between charges on the surface becomes not only smaller than Bjerrum length l_B but also smaller than ion size.